

COMMISSIONING OF CURRENT STRIPS FOR ELLIPTICALLY POLARIZING UNDULATORS AT NSLS-II*

Y. Hidaka[†], O. Chubar, T. Tanabe, Brookhaven National Laboratory, Upton, NY, USA
C. A. Kitegi, Synchrotron SOLEIL, GIF-sur-YVETTE, France

Abstract

Most of the Elliptically Polarizing Undulators (EPU) at NSLS-II are equipped with current strips (or flat wires), attached to their vacuum chambers. These strips compensate the dynamic field integrals of the EPU to minimize undesirable nonlinear beam dynamics effect that can lead to reduction in injection efficiency and beam lifetime. For each EPU, we measured the field integrals of the insertion device alone, the current strips alone, and both, while creating horizontal bumps of different amplitudes at the straight section to assess the effectiveness of the compensation provided by the design current values for the strips. The commissioning results of these current strips are reported in this article.

INTRODUCTION

The National Synchrotron Light Source II (NSLS-II) is a double-bend-achromat 3-GeV storage ring commissioned in 2014 at Brookhaven National Laboratory [1]. There are currently a total of 6 EPUs in user operation. Except for one refurbished EPU at Cell 7, all the EPUs (one at Cell 2, two each at Cell 21 and 23) were built with current strips (CS), i.e., flat wires attached to the top and bottom of the vacuum chamber. We employ these current strips for active compensation of the dynamic field components because passive methods like L-shim cannot correct the field for all the available polarizations [2-7].

Without this compensation, the uncompensated second-order kicks act effectively as nonlinear multipoles that can significantly degrade nonlinear beam dynamics, resulting in reduced injection efficiency and/or beam lifetime. Figure 1 shows an example of dynamic aperture collapse in 6-D tracking simulations for NSLS-II using Tracy [8].

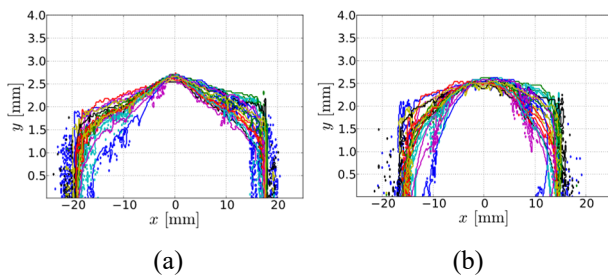


Figure 1: NSLS-II dynamic apertures via simulations with current strips (a) collapse when current strips are turned off (b). Different lines are the results of different seeds to generate random errors in multipoles and alignments.

MEASUREMENT METHODS

To characterize the dynamic field integrals of the ID itself (“ID only”), those of the CS alone (“CS only”), and those of the ID and the current strips (“ID+CS”), we performed field integral measurements with large horizontal bumps. At a straight section where the ID is located, we create horizontal offset bumps (i.e., zero angle bumps) with different amplitudes. For each bump, a reference orbit is first recorded with the ID gap fully open and the CS currents are zeroed. For “ID only”, the EPU gap and phase are set to the values of interest with CS off. For “CS only”, the ID stays fully open, but the power supplies for CS are set to the values pre-computed by RADIA [9] using Tikhonov regularization method to compensate the intrinsic 2nd-order kicks from the ID. For “ID+CS”, the ID state is changed to a state of interest, while the CS power supplies are set to the corresponding correction values. After these state changes, a new orbit is recorded. In a lattice model [8, 10], the horizontal kick angles of virtual kick elements placed at both ends of the ID element are adjusted by minimizing the difference between the simulated orbit distortion and the measured orbit distortion from the reference. By simply summing the fitted upstream and downstream virtual kick angles θ_x^{US} and θ_x^{DS} , we can estimate the first field integrals by the following equation:

$$\frac{I_{1y}}{B\rho} = \frac{\int B_y(s)ds}{B\rho} = \Delta\theta_x = \theta_x^{US} + \theta_x^{DS}.$$

Note that the measured I_{1y} contains the effects from both the first-order effect that can be measured with flip coils [11] and the second-order effect that results from the electron’s wiggling motion and hence can be measured only with electron beam [12]:

$$\int B_y(s)ds \approx -\frac{L}{2k^2B\rho} B_y(x_i) \cdot \frac{dB_y(x_i)}{dx},$$

where L is the device length, $k = 2\pi/\lambda$ and λ is the period length. x_i is the horizontal coordinate at the ID entrance.

This measurement procedure (“alternating”) was quite time consuming: 1) Open the ID; 2) Create a large horizontal bump and measure the bumped orbit as a reference; 3) Close the ID and measure an orbit; 4) Repeat the steps above for each bump. It takes long because creation of each bump needs fine tuning, as it is not easily reproducible due to the hysteresis of the orbit correctors. In addition, the ID needs to be opened and closed repeatedly, which takes up to a few minutes for each round trip.

* Work supported by U.S. DOE under Contract No. DE-SC0012704.

[†] yhidaka@bnl.gov

Later a new “constant” method was used to significantly speed up the measurements: 1) First make all the horizontal bumps (with the ID open); 2) Cycle the bump settings several times to condition; 3) With the ID open, cycle through the bumps once while measuring orbits as the reference orbits; 4) Close the ID and cycle through the bumps once while measuring orbits. This method is called “constant” because the ID stays constantly open or closed during orbit measurements, which eliminates the significant portion of the measurement time. Step 2 is performed to have reproducible bumps. Step 1 still requires a substantial amount of time, but the series of bumps once generated can be re-used for any number of different gap/phase states. This is not the case with the “alternating” method because of the somewhat random nature of the bump fine-tuning process breaking cyclical setpoint changes, hence requiring fine tuning for each scan.

With the alternating method, only spot checks were performed as it took ~ 1 hour per bump scan even after the bumps were roughly set up without fine tuning. With the constant method, a 1st-field integral curve shown in Fig. 2 can be obtained with only ~ 10 minutes (excluding the initial setup time to generate the bump series).

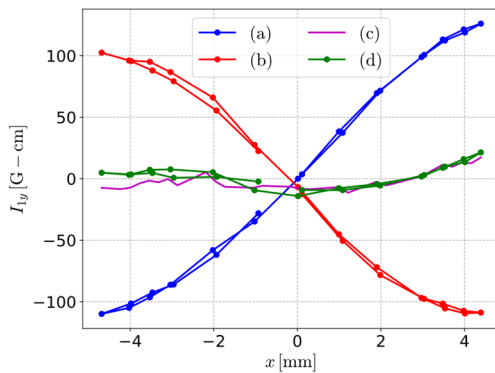


Figure 2: Vertical first field integral measurements for ESM EPU57 at Cell 21 in Linear Vertical (LV) mode with the gap of 16 mm and phase of +28.5 mm: (a) ID closed in LV with CS off; (b) ID open + CS 80%; (c) curves (a) + (b); (d) ID closed in LV with CS 80%.

RESULTS

Figure 2 shows a typical direct measurement of dynamic field integrals from an EPU, shown as the blue curve (a). The red curve (b) shows the field integral generated when the pre-computed compensation current values for CS were applied, while the ID is fully open. This curve should be ideally close to the vertically flipped version of the blue curve. If so, this results in near perfect cancellation of the ID’s dynamic field integrals measured when the ID is closed, and the CS was turned on. This is experimentally demonstrated as the nearly flat green curve (d). The magenta curve (c) is simply the sum of (a) and (b), which is almost identical to (d). This confirms linear superposition of the field integral from the ID and that from the CS.

From the measured field integral curves like Fig. 2, we found that applying 100% correction of the pre-computed

CS current values overcompensate for most of the CS-equipped EPUs, as in [4]. For SIX EPU57 at Cell 2, 70% correction was found optimal, while 80% and 75% were best for ESM EPU57 and EPU105, respectively, at Cell 21.

To investigate this discrepancy by potential misalignments of CS wires, we measured the “response matrix” of the CS channel currents vs. the first field integral curves for ESM57 and ESM105 at Cell 21. For each bump scan, we only activate one CS channel with a certain amount of current and obtain vertical and horizontal field integral curves as circles shown in Fig. 3. The dotted lines are the field integral curves predicted by the magnetic field formula [13] from an infinitely-long, thin straight wire based on Biot-Savart law, assuming the CS wires are located at the design positions and the current readings are accurate:

$$\vec{B} = \frac{\mu_0 I (-y'_0 \hat{x} + x'_0 \hat{y})}{2\pi(x'_0{}^2 + y'_0{}^2)},$$

where $x'_0 = x_{\text{obs}} - x_{\text{src}}$ and $y'_0 = y_{\text{obs}} - y_{\text{src}}$, and the subscripts “obs” and “src” denote the observation and source points, respectively. Each solid line in Fig. 3 corresponds to simulated vertical and horizontal field integral curves that fits the measured curves best after adjusting the transverse positions of the CS wires for a different assumed CS length. The base ID length for ESM57 and ESM105 were 1.4 and 2.8 m, while the CS length from the drawings was 1.486 and 2.931 m, respectively. For the fitting, lengths up to +30% from the base ID length were considered.

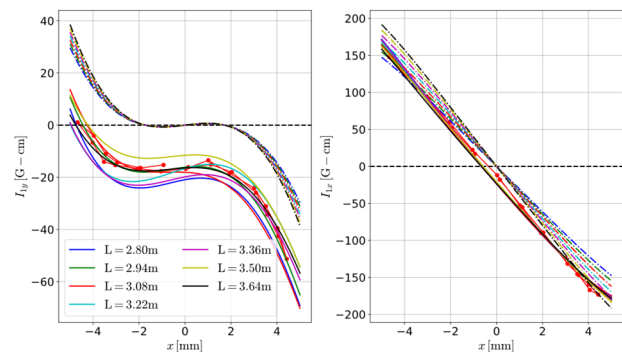


Figure 3: Measured “response curves” (circles) with simulated curves (solid lines) with the CS wire transverse positions as fitting parameters for different assumed wire lengths. Dotted lines represent the curves with the design wire locations.

Note that the CS at NSLS-II are all diagonally connected in series as shown in Fig. 4. Therefore, we cannot use the ratio matrix method in [13] to estimate CS misalignments as it requires each wire being powered independently.

Figures 5 and 6 show the estimated CS wire positions for ESM57 and ESM105, respectively. The squares represent the design positions of the wires, while the circles are the best estimated positions for different assumed CS lengths, the minimum of which corresponds to the base ID length and denoted by the triangles.

Content from this work may be used under the terms of the CC BY 3.0 licence (© 2021). Any distribution of this work must maintain attribution to the author(s), title of the work, publisher, and DOI

For both cases, the horizontal zero position defined by zero positions of the nearby ID beam position monitors (BPMs) appear to be off by 0.5 mm from the center of the current strips. The figures' horizontal axes are already shifted by this amount. The zero positions of ID BPMs are defined by the zero positions of the nearby arc BPMs, which are defined by the beam-based alignment (BBA) to the nearest quadrupoles. Thus, it is not surprising to see this offset as the quadrupole centers are not guaranteed to be perfectly aligned with the ID/CS horizontal center line.

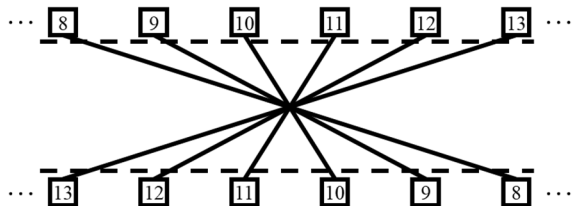


Figure 4: Cross-sectional view of CS (e-beam moving into the paper). The squares represent the positions of CS wires with channel numbers. The dotted lines indicate the top and bottom walls of the vacuum chamber, while the solid lines connecting wires indicate electrical connection in series (wires not physically going through the chamber).

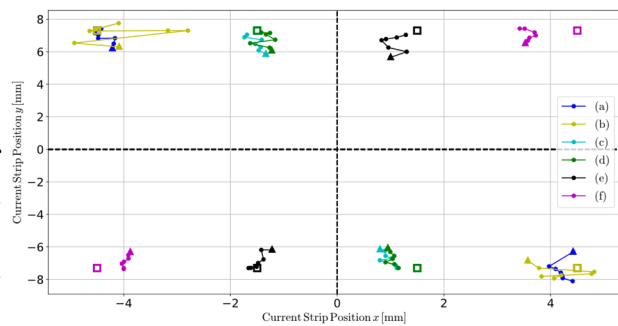


Figure 5: CS wire position for ESM 57 estimated from the measured field integrals for (a) & (b): Ch. 9 ± 3 A, (c) & (d) Ch. 10 ± 3 A, (e) Ch. 11 ± 3 A, and (f) Ch. 12 ± 3 A. The horizontal positions are shifted by +0.5 mm with respect to the ID BPM zero positions.

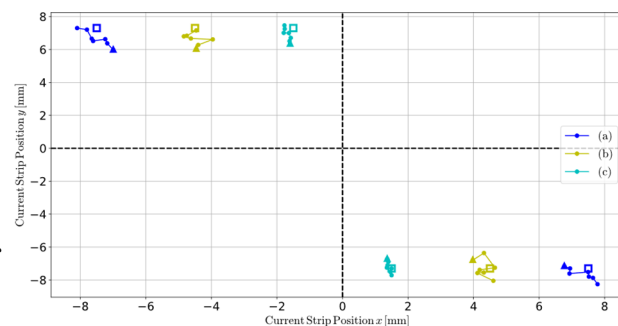


Figure 6: CS wire position for ESM 105 estimated from the measured field integrals when Channels 8 (a), 9 (b), and 10 (c) were applied + 3 A. The horizontal positions are shifted by + 0.5 mm with respect to the ID BPM zero positions.

In both cases, if we consider the maximum case for 130% of the base ID length (1.4 and 2.8 m), the estimated vertical separation is close to the design value of 14.6 mm. However, this assumption is probably too unrealistic. For the minimum length considered (i.e., base ID length), which is very close to the physical wire length in the drawing, the vertical channel separation appears closer than the design value by almost 1 mm. This would require the vacuum chamber height to be shorter than design and remains to be checked.

Another thing to note from Figs. 5 and 6 is that the horizontal channel separation for ESM57 appears closer than the design value of 3 mm by a few hundred μm .

The downstream CSX EPU49 at Cell 23 was the only exception in that it did not require any scaling from the pre-computed compensation values to achieve good correction. However, the upstream CSX EPU49 exhibited an abnormal curve in the device field integrals as shown in Fig. 7, which resulted in very poor compensation. This might be either due to the horizontal center of the ID and that of CS not being aligned by ~ 1.5 mm or due to a known physical damage incident to this device before installation. The CS for these EPUs are currently disabled, while we investigate ways to remedy this problem.

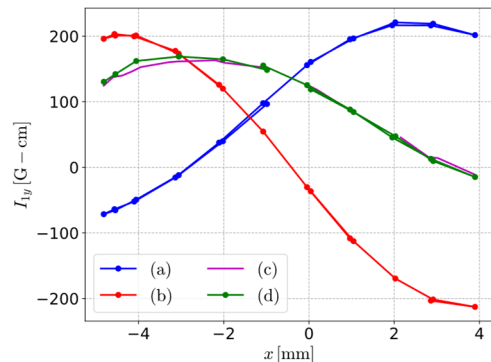


Figure 7: Vertical first field integral measurements for upstream CSX EPU49 at Cell 23 in Linear Vertical (LV) mode with the gap of 12 mm and phase of + 24.6 mm: (a) ID closed in LV with CS off; (b) ID open + CS 100%; (c) curves (a) + (b); (d) ID closed in LV with CS 100%.

CONCLUSION

We have successfully commissioned the current strips (CS) for most of the EPUs installed at NSLS-II. We devised an efficient method to directly measure the first field integrals with a series of large horizontal bumps to confirm the effectiveness of the current strip compensation of dynamic field integrals of EPUs. From these measurements, it was found that the pre-computed CS compensation currents were generating field integrals larger than expected by 20-30% for many of our EPUs. From the measured response field integral curves for different CS wires, the wire position deviations were estimated. For realistic CS lengths, the vertical wire separation appeared closer than the design value by 1 mm. Further investigations are needed to confirm the source of the unexpectedly large field integrals generated by the CS wires.

REFERENCES

- [1] G. M. Wang *et al.*, “NSLS-II SR Commissioning Report”, BNL, Upton, NY, USA, Rep. NSLSII-ASD-TN-168; BNL-211142-2019-TECH, Apr. 2015.
- [2] J. Bahrtdt and G. Wüstefeld, “Symplectic tracking and compensation of dynamic field integrals in complex undulator structures”, *Physical Review Special Topics - Accelerators and Beams*, vol. 14, no. 4, p. 040703, 2011. doi:10.1103/physrevstab.14.040703
- [3] J. Bahrtdt, W. Frentrup, A. Gaupp, M. Scheer, and G. Wüstefeld, “Active Shimming of the Dynamic Multipoles of the BESSY UE112 APPLE Undulator”, in *Proc. 11th European Particle Accelerator Conf. (EPAC’08)*, Genoa, Italy, Jun. 2008, paper WEPC097, pp. 2222-2224.
- [4] B. Singh *et al.*, “Active Shimming of Dynamic Multipoles of an APPLE II Undulator in the Diamond Storage Ring”, in *Proc. 4th Int. Particle Accelerator Conf. (IPAC’13)*, Shanghai, China, May 2013, paper TUPWO057, pp. 1997-1999.
- [5] Q. L. Zhang, B. C. Jiang, S. Q. Tian, Z. T. Zhao, and Q. G. Zhou, “Study on Beam Dynamics of a Knot-APPLE Undulator Proposed for SSRF”, in *Proc. 6th Int. Particle Accelerator Conf. (IPAC’15)*, Richmond, VA, USA, May 2015, pp. 1669-1671.
doi:10.18429/JACoW-IPAC2015-TUPJE022
- [6] T. Tanabe *et al.*, “Latest experiences and future plans on NSLS-II insertion devices”, *AIP Conference Proceedings*, vol. 1741, p. 020004, 2016. doi:10.1063/1.4952783
- [7] J. Bengtsson, O. V. Chubar, C. A. Kitegi, and T. Tanabe, “Control of Nonlinear Dynamics by Active and Passive Methods for the NSLS-II Insertion Devices”, in *Proc. 3rd Int. Particle Accelerator Conf. (IPAC’12)*, New Orleans, LA, USA, May 2012, paper MOPPP088, pp. 759-761.
- [8] J. Bengtsson, E. Forest, and H. Nishimura, *Tracy User Manual*, Internal SLS document, PSI, Villigen, Switzerland, 1997.
- [9] O. Chubar, P. Elleaume, and J. Chavanne, “A 3D Magneto-statics Computer Code for Insertion Devices”, *Journal of Synchrotron Radiation*, vol. 5, pp. 481-484, 1998. doi:10.1107/s0909049597013502
- [10] M. Borland, “elegant: A Flexible SDDS-Compliant Code for Accelerator Simulation”, in *Proc. 6th International Computational Accelerator Physics Conf. (ICAP 2000)*, Darmstadt, Germany, Sep. 2000, paper LS-287. doi:10.2172/761286
- [11] T. Tanabe *et al.*, “Insertion devices at the national synchrotron light source-II”, *Synchrotron Radiation News*, vol. 28, pp. 39-44, 2015.
doi:10.1080/08940886.2015.1037682
- [12] J. Safranek, C. Limborg, A. Terebilo, K. I. Blomqvist, P. Elleaume, and Y. Nosochkov, “Nonlinear dynamics in a SPEAR wiggler”, *Physical Review Special Topics - Accelerators and Beams*, vol. 5, p. 010701, 2002. doi:10.1103/physrevstab.5.010701
- [13] W. A. Wurtz and Q. L. Zhang, “Alignment of Current Strips at the Canadian Light Source”, in *Proc. 9th Int. Particle Accelerator Conf. (IPAC’18)*, Vancouver, Canada, Apr.-May 2018, pp. 1342-1345.
doi:10.18429/JACoW-IPAC2018-TUPMF040